Egyptian Journal of Chemistry

http://ejchem.journals.ekb.eg/

Effect of Annealing on Optical Crystallinity and Gas Sensing Characteristics of Tin Monosulfide Thin Films Deposited by DC Sputtering

Dunia F. T. AL-Ani [a]*, Bushra Khamas Abbas[b]

[a,b,] *Department of Physics, College of Science, Mustansiriyah University, Baghdad, Iraq*

Abstract

Tin monosulfide (SnS) was prepared via DC magnetron sputtering on glass substrates and annealed at two temperatures (200, 300) ºC. The annealing effect on crystallinity, optical and gas sensing characteristics of Tin monosulfide films were examined. The morphology and structure of creating SnS thin films have been researched via scanning electron microscopy (SEM), X-ray diffractions (XRD), and Atomic Force Microscopy (AFM). XRD results explain that the increasing annealing temperature from 200ºC to 300ºC caused an increase in crystallite size, while the Microstrain and the dislocation density were reduced. SEM showed that the increasing in the SnS cluster distribution with particle size increases with increasing the annealing temperature. Optical properties prove that the energy gap decreases 2.185 eV to 1.967 eV as the annealing temperature increases from 200oC to 300oC, and the annealed samples exhibited enhanced gas sensitivity up to 75%.

Keywords: Particle size, Tin monosulfide, A post anneal, Energy gap, Reduced gas, Gas sensor;

1. Introduction

The most appealing and ideal contender for an energy carrier and future fuel is hydrogen [1]. The capacity for monitoring and detecting hydrogen gas is a typical requirement in this field, yet hydrogen gas sensors which might consistently identify hydrogen over many oxygen and moisture concentrations are presently unavailable [2]. For instance, in the chemical sector, there are several variants of hydrogen bulk sensors [3]. Concentration monitoring of hydrogen is highly critical for the application of fuel cells and for the scenario where hydrogen is an undesired pollutant. Thin film sensors include Pd-catalyzed field effect transistors (FETs) and chemo-resistive Pd alloy resistors [4]. Other hydrogen sensors, depending on various materials, have distinct operating principles and types. Optical fibers [5], thermo-electric sensor wire coated with Pd [6], piezoelectric type [7], Schottky and MIS diodes [8, solid electrolytes [9], polymers [10], potentiometric and amperometric sensors [11], fullerene sensors and carbon nanotube [12], graphite oxide, and various metal oxides are among them [13, 14].

2. Experimental

By using the DC magnetron sputtering approach, thin films of Tin monosulfide have been produced on well-cleaned glass substrates (Super River w. Germany) kept at a range of temperature between 40 ºC and 50 ºC, which represents sputter chamber temperature. In the sputter dawn setup, a tin monosulfide target (1:1 99.99% purity, which has been provided by the Nuclear Fuel Complex in India) with a thickness of 3 mm and diameter of 50 mm has been utilized as a sputter target for film's deposition. Thickness and deposition rate were both controlled via a crystal sensor and held at (0.1 – 0.2) /Sec (FTM-2000). The substrate and target were separated by a distance of (100 mm). Using a turbo molecular

combination and rotary oil pump, the sputter chamber has been evacuated to a 4.10 x 10^{-6} torr base pressure. A digital Pirani - Penning gauge (adixen ACS2000) combination was utilized for measuring the pressure in the sputter chamber. The films were deposited using Argon 99.999% purity as a sputter gas. With the help of a gas mass flue controller (Ailcat scientific), Argon gas was able to enter the chamber at a partial pressure of (3.2×10^{-3} torr). To supply the 200 W sputter target, (13.5KHz) RF power (TORR INTERNATIONAL, INC.CRC-600) was utilized. The XRD approach (Shimadzu 6-2000, with cuk radiation that has a wave-length=0.15406nm) has been utilized to determine the crystal structure of deposited films. (S-4160) Hitachi (college of engineering and communications, Iran) was used to examine the surface microstructure. The gas sensor features are conducted and manufactured locally and include a vacuum-tight stainless steel cylindrical testing chamber with a height of 16cm and a diameter of 20cm, with a removable bottom base and an O-ring sealed bottom base. The chamber's effective volume is 5440 cm^3. It has an inlet for test gas and air admittance valve for ambient air once it has been evacuated.

3. Results and dissection

XRD patterns of manufactured SnS films which have been deposited on glass through DC sputtering and post-annealed at (200o and 300) °C, the samples were annealed for two hours Figure 1. Films that were deposited on glass and annealed at T =200oC and 300 °C showed polycrystalline nature with prefer reflection along (131) plan corresponding to the 2Θ 39.2°, thus peak intensity increased as the temperature of the substrate increased up to 300°C, and other minor peaks (111), (211) and (121) that corresponding to 2Θ (31.55°, 45.5° and 51.1°) present in both the tow samples matched with standard peaks (JCPDS card 33-1375) [15]. The degree of crystalline and the crystallite size that were calculated by Debby Scherrer formula (1) [16], increased from 22 nm to 26 nm for the preferred reflection because of the heat treatment process [17]. Also, Figure 1a,b shows that the dislocation density and the microstrain decreased as the annealing temperature increased due to crystalline improving the variety of grain size and structural parameters are listed in Table 1.

$$D= (k\lambda)/(\beta\cos\theta) \quad (1)$$

In which, k represents 0.94 constant for (cukα), β represents full width at half-maximum (FWHM)

intensity in radians. (θ) represents Bragg angle of preferred peak.
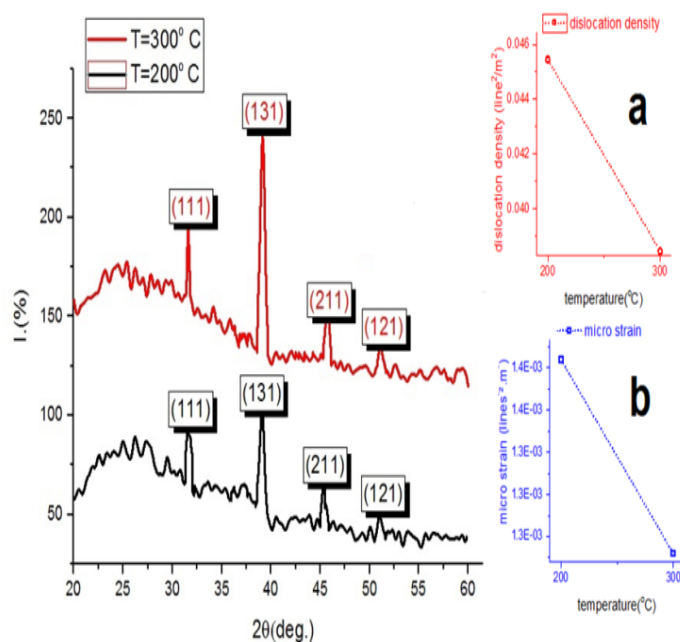

Fig. 1: XRD spectra regarding the SnS thin films deposited by DC sputter (a) dislocation density (b) microstrain.

SEM is a convenient technique for studying the nanostructure of SnS thin films which were deposited on glass substrates. Figure 2 shows the SEM images of SnS thin film which were deposited at annealing temperatures, 200°C and 300°C. Whereas SEM images revealed the growth of oriented randomly and multi-grains, which were uniformly distributed over the surface. From the micrograph, it is obviously seen that grain size and the amount of Cluster increase, thus gets smaller with uniform distribution with increasing of substrate temperature that has been identified in AFM investigations. The creation of large grains is due to a combination of small grains and reorganization of the increasing availability of thermal energy at higher, which results in increased grain size.

AFM which pictures 2Dview and average grain diameter distribution of SnS thin films grown at two typical post annealing are illustrated in figure 3. The average grain size as well as RMS value of surface roughness were increased with an increase in the

annealing temperature, the variation of surface roughness and grain size are listed in Table 2.

Table 1. Structural Parameters of the SnS Thin Film Prepared DC Sputtering.

| Annealing temperature	(hkl) plan	2Θ (°)	FWHM (°)	I (%)	D (nm)	Dislocation Density $\delta \times 10^{15}$ (line²/m²)	Micro strain $\varepsilon \times 10^{-3}$ (lines⁻².m⁻)
200°C	(111)	31.55	0.266	31	30.12	0.033	1.11E-03
	(131)	39.2	0.356	42	22.3	0.045	1.46E-03
	(211)	45.5	0.306	25	25.05	0.040	1.23E-03
	(121)	51.1	0.375	17	20.61	0.050	1.47E-03
300°C	(111)	31.44	0.296	29	27.48	0.037	1.24E-03
	(131)	39.15	0.301	70	26.21	0.038	1.23E-03
	(211)	45.45	0.348	23	2216	0.045	1.40E-03
	(121)	51.21	0.312	16	24.23	0.042	1.22E-03
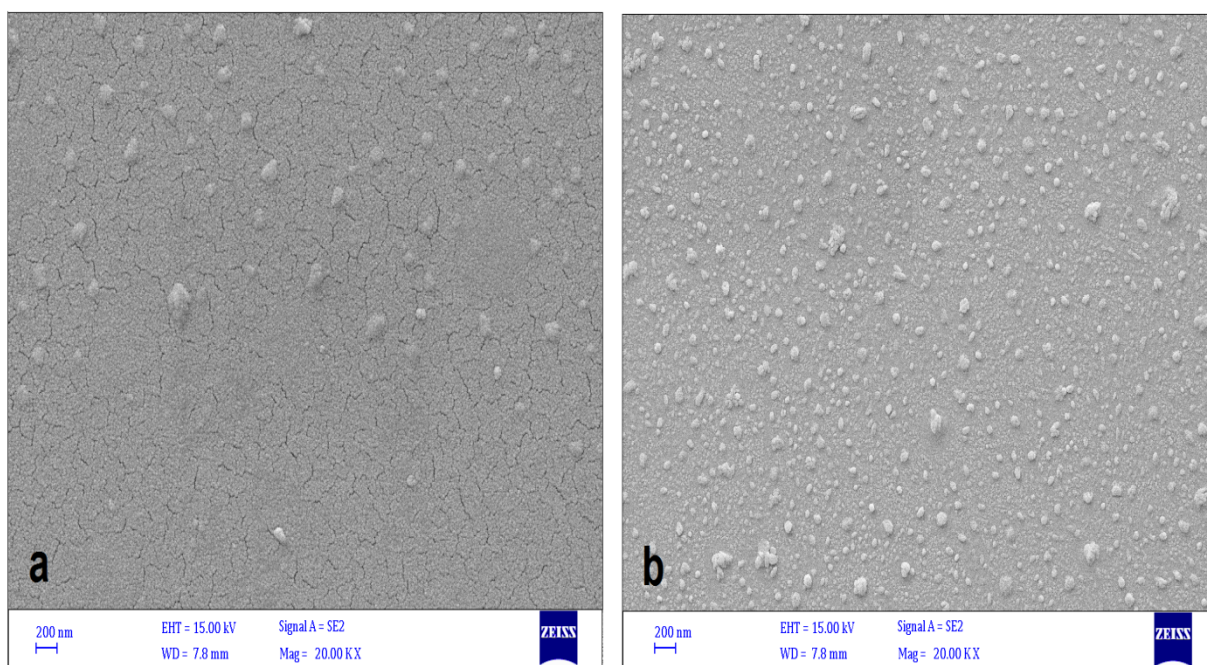
Fig. 2. SEM micrographs of SnS thin film (a) annealed at 200°C and (b) annealed at 300°C.

AFM which pictures 2Dview and average grain diameter distribution of SnS thin films grown at two typical post annealing are illustrated in figure 3. The average grains size as well as RMS value of surface roughness were increased with an increase in the annealing temperature, the variation of surface roughness and grain size are listed in Table 2.
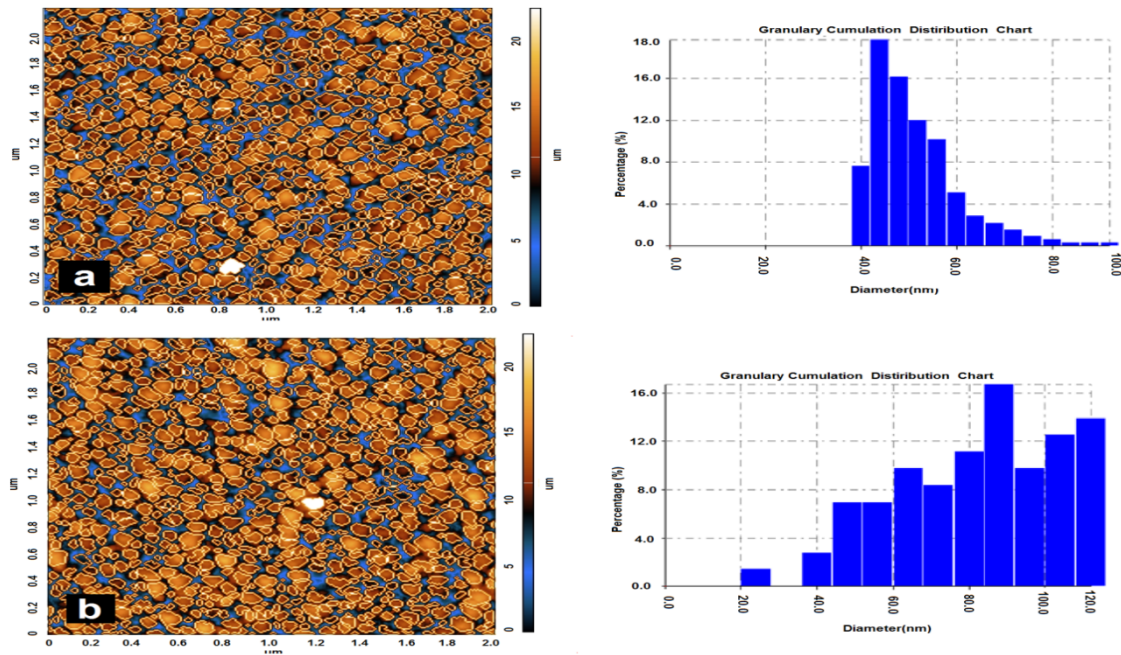
_____

Fig. 3. AFM images and granularity accumulation distribution chart of the SnS thin film
annealed at (a) 200ºC (b) 300ºC.

Table 2: Mean grain size, Roughness average and
RMS of SnS thin film

Substrate temperature	Average size of the grain (nm)	Roughness average (nm)	RMS (nm)
200 ⁰C	65	1.98	2.6
300 ⁰C	90	1.45	2.35

Figure 4 exhibits the transmittance spectrums of SnS nanoparticles deposited via DC magnetron sputtering. It is so remarkable that decreasing in the transmittance from its maximum value (80 %) to (73 %) as the substrate annealing temperature increase from 200ºC to 300ºC, with constancy of transmittance in the visible and near infrared region

(330 – 900), due to the increases in the crystalline size from (22.3nm) to (26.21 nm). And we can note the shift in the absorption edge of the word of longer wavelength is due to crystalline increasing. The optical band gap calculated by the equation [18].

$$\alpha h\vartheta = A\left(h\vartheta - E_g\right)^n \qquad (2)$$

Where E_g represents the semiconductor's band gap, α represents the coefficient of the absorption, $h\vartheta$ represents photon energy, A is constant and n can take as (2) corresponding allowed indirect transition [19].

Where E_g represents the semiconductor's band gap, α represents the coefficient of the absorption, $h\vartheta$ represents photon energy, A is constant and n can take as (2) corresponding allowed indirect transition [19].
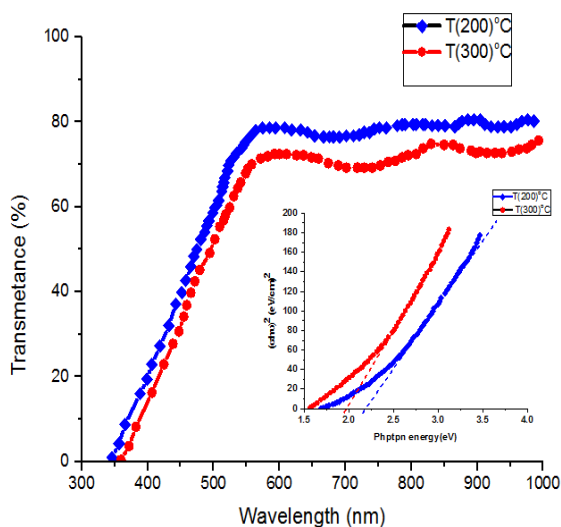
Fig. 4. Optical transmittance of SnS thin films and $(\alpha h v)^2$ versus photon energy plot.

Fig. 5. A Dynamic Resistance Change of SnS Films for Different Concentration Values for H_2 Gas at 150ºC Operating Temperature.

Figure 5 depicts the dynamic resistance change related to the SnS films which are prepared via DC magnetron sputtering as well as the Ag electrode material which is deposited via screen printing method on the glass substrate as illustrated in Figure 5a with a 150oC operating temperature and exposure to various concentrations of H_2 gas (300, 350, and 400) ppm as a function of operating time. Since SnS is an n-type semiconductor, its electric resistance drops when hydrogen gas, a reducing gas, is present [20]. This drop can be explained by the fact that electrons are travelling across the conduction band, which results in increasing the density of majority charge carriers (electrons) at gas-solid interface. With an increase in the density of hydrogen ions on the surface, the potential barrier for electrons reduces. The electrical resistivity value decreases due to the potential barrier and depletion layer; this value is highly reliant upon the concentration of the deposited Hydrogen ions on the surface [21].
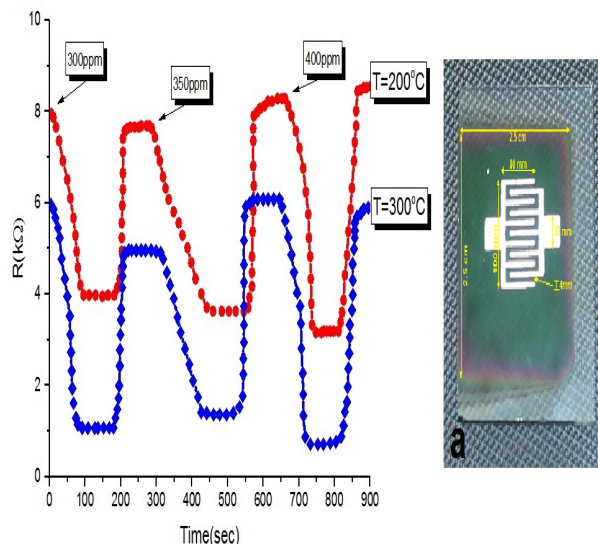
The sensitivity of SnS films was shown in figure 6 and estimated by using the formula (3).

$$\text{Sensitivity} = S = \frac{\Delta R}{R_g} = \left| \frac{R_a - R_g}{R_a} \right| \times 100\% \qquad (3)$$

In which R_a represents the film sensor resistance in presence of air, R_g represents the resistance of film sensor in the presence of gas.

It can be seen increasing of sensitivity with increasing of substrate temperature and gas concentration a figure 6a, b. The sensor's lifetime is shortened as a result of the high substrate temperature, and increased resistance necessitates more electricity for operation. The interactions between the sensor surface and target gas determines the sensitivity regarding the metal sulfide sensor. Generally, increasing the operating temperature produces a more homogeneous surface with uniform roughness, resulting in a larger surface area and a higher possibility of vapor gas reaction. Sensing is widely understood to be a surface process governed mostly by desorption and adsorption species [22]. The adsorption type of Hydrogen molecules is chemisorption at high temperature degrees and physisorption at lower temperature degrees, which explains the changes in sensitivity with gas concentration [23]. Figures 6-a, b illustrate the recovery time and response time, which might be directly from figure 5 and displayed as a function of gas concentration (ppm), with response time

increasing from (40 to roughly 42) Sec. The increased response time could be related to the greater number of unoccupied sites for gas adsorption on thin films [24]. The response time values in all SnS films to H_2 gas are convergent, with the maximum response time observed for the sample annealed at (300) ºC. In the case when the H2 molecules adsorb on the metal sulfide's surface, the conduction band (E_c) receives electrons, trapping the hole at the surface. This is going to result in the formation of an electron-depleted area. As the depletion zone of the SnS gas sensor decreases while reacting with H_2 gas, and the depletion layer extends as SnS reacts with reduced, this condition will result in the resistance value to drop as the gas concentration grows. The recovery time for the sample annealed at 200ºC was reduced from 90 seconds to 80 seconds in Figure 6-a, b. For the substrate annealed at 300ºC and increasing up to H_2 gas concentration increases, because of the sensor saturation by the target gas, as well as a variation in structural qualities that may occur as a result of the operating temperature.
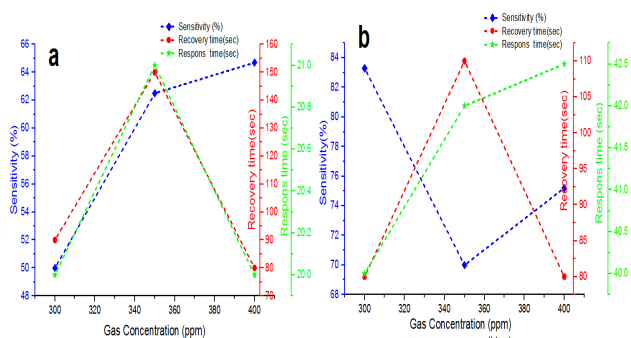

Fig. 6. (a) Sensitivity, Recovery time and response time for SnS Films annealed at 200ºC for Different Concentrations of H_2 Gas (b) Sensitivity, Recovery time and response time for SnS Films annealed at 200ºC for Different Concentrations of H_2 Gas.

4. Conclusions

SnS prepared films by DC magnetron sputter, shows nano-polycrystalline nature with a preferred (131) plane. Increasing the annealing substrate temperature from 200oC up to 300 ºC lead to an increase in the both SnS particles size and cluster number on the film surface, which returned clearly to enhance the sensing properties of hydrogen gas through an increase in the sensitivity value up to 75% with variation both of substrate annealing temperature and gas concentration.

Conflicts of interest

No conflict of interest

References

[1] Eguchi K., Concept of Energy Carrier, Candidate Materials, and Reactions, book, 2016.

[2] Shin W., Nishibori M., Houlet L. F., Tajima K., Itoh T., Izu N., Matsubara I., Robust ,Thermoelectric Hydrogen Sensors with Ceramic Catalyst. WHEC, 16, 13-16, (2006).

[3] Feng P., Shao F., Shi Y. and Wan Q., Gas Sensors Based on Semiconducting Nanowire Field-Effect Transistors. Sensors, 14, 17406-17429, (2014).

[4] Liu X., Cheng S., Liu H., Hu S., Zhang D. and Ning H., A Survey on Gas Sensing Technology. Sensors, 12(7): 9635–9665, (2012).

[5] Peters K., Polymer optical fiber sensors, a review. IOP Publishing Ltd, 20, 1, (2010)

[6] Zhu L., Wang L., Xue F., Chen L., Fu J., Feng X., Li T. and Wang Z. L., Piezo- Phototropic Effect Enhanced Flexible Solar Cells Based on n-ZnO/p-SnS Core–Shell Nanowire Array. Adv. Sci., 4, 1-7, (2017) .

[7] Chaki S., Joshi H. J., Pravinkumar T. J., Study of SnS2 thin film deposited by spin coating technique. Mater. Res. Express, 4, 764 02, (2017).

[8] Chand S. and Kumar J., Current-voltage characteristics and barrier parameters of Pd2Si/p-Si (111) Schottky diodes in a wide temperature range. Semicond Sci Technol., 10 (12), 1680, (2016).

[9] VasanthiPillay V. and Vijayalakshmi K., Effect of rf power on the structural properties of indium tin oxide thin film prepared for application in hydrogen gas. Sensor, 24(6), 1895–1899, (2013).

[10] Grieshaber D., MacKenzie R., Vörös J. and Reimhult E., Electrochemical Biosensors - Sensor Principles and Architectures. Sensor, 8(3), 1400-1458, (2008).

[11] Myung Y., Myung J. D., Cho Y. J., Sung K. H. and Park J., Nonenzymatic Amperometric Glucose Sensing of Platinum, Copper Sulfide, and Tin Oxide Nanoparticle-Carbon Nanotube

Hybrid Nanostructures. J. Phys. Chem. C, 113(4), 1251–1259, (2009).

[12] Chen J.G., NEXAFS investigations of transition metal oxides, nitrides, carbides, sulfides and other interstitial compounds. Surf. Sci. Rep. 30(3), 1-152, (1997).

[13] Mukherjee A., Mitra P., Structural and optical characteristics of the SnS thin film prepared by SILAR. Materials Science-Poland, 33 (4), 847-85, (2015).

[14] Cifuentes C., Botero M., Romero E., Calderón C., Gordillo G., Optical and structural studies on SnS films grown by co-evaporation. Braz. J. Phys. 36 (3), 1046- 1049, (2006).

[15] Zi T., Bharath K.Y. and Ha G., Investigation on quickly deposited SnS thin films by Chemical Bath Deposition. Semicond. Sci. Technol. 18, 501-505, (2003).

[16] Barsan N. and Weimar U., Fundamentals of Metal Oxide Gas Sensors. IMCS– The 14th International Meeting on Chemical Sensors (2012).

[17] hoonnoho S., Kwonchoi B., Heehan C., Hoonkang S., Yong H. J., Effects of Heat Treatments on Microstructures and Mechanical Properties of Dual Phase Steels For High Temperature Strength. Nucl. Eng. Technol. 45(6), 821-826, (2013).

[18] Mohammed R. S., Aadim K. A., Ahmed Kh. A., Synthesis of CuO/ZnO and MgO/ZnO Core/Shell Nanoparticles with Plasma Jets and Study of their Structural and Optical Properties. Karbala International Journal of Modern Science, 8(2), 88-97, (2022).

[19] Kazmarski L. and Clark A. H., Polycrystalline and Amorphous Thin Films and Device. Edited by Lawrence Academic Press, New York, (1980).

[20] Wetchakun K., Semiconducting Metal Oxides as Sensors for Environmentally Hazardous Gases. Sens. Actuators B Chem. 160(1), 580–591(2011).

[21] Aslani A., Oroojpour V. and Fallahi M., Sonochemical Synthesis, Size Controlling and Gas Sensing Properties of NiO Nanoparticles. Appl. Surf. Sci. 257(9): 4056-4061, (2011).

[22] Ahlers S., Muler S. G. and Doll T., A Rate Equation Approach to the Gas Sensitivity of the Thin Film Metal Oxide Materials. Sens. Actuators B Chem., 107 (2), 587-599. (2005)

[23] Batzill M. and Diebold U., The Surface and Materials Science of Tin Oxide. Prog. Surf. Sci., 79, 47–154, (2005).

[24] Giraldi T.R., Escote M.T., Bernardi M.I.B., Leit V.R., Effect of Thickness on the Electrical and Optical Properties of Sb Doped SnO_2 (ATO) Thin Films. J. Electroceramics, 13, 159–165, (2004).